minerals

MDPI

Article

Mineralogy and Processing of Hydrothermal Vein Quartz from Hengche, Hubei Province (China)

Min Lin *, Zhenyu Pei and Shaomin Lei

School of Resources and Environmental Engineering, Wuhan University of Technology, Wuhan 430070, China; zhypei@163.com (Z.P.); shmlei@163.com (S.L.)

* Correspondence: 208726@whut.edu.cn; Tel.: +86-027-8788-5647

Received: 19 July 2017; Accepted: 31 August 2017; Published: 2 September 2017

Abstract: Quartz occurs in many geological materials, and is used in numerous industrial fields as a raw material. Mineralogy and the processing of hydrothermal quartz were studied by optical microscope, electron probe microanalysis, scanning electron microscope, inductively coupled plasma-optical emission spectrometry, and inductively coupled plasma mass spectrometer. A combination of the geological occurrence of the quartz deposit, mineralogical studies, and the processing technologies of the hydrothermal quartz was accomplished. The results show that impurities within the quartz mainly include muscovite, hematite, apatite, and secondary fluid inclusions. The main chemical impurities are Al (353 $\mu g \cdot g^{-1}$), K (118 $\mu g \cdot g^{-1}$), Fe (61.2 $\mu g \cdot g^{-1}$), P (15.5 $\mu g \cdot g^{-1}$), Na (13.4 $\mu g \cdot g^{-1}$), Mg (11.8 $\mu g \cdot g^{-1}$), Ti (8.31 $\mu g \cdot g^{-1}$), and B (10.8 $\mu g \cdot g^{-1}$). Based on these results, a combined process consisting of calcination and fluoride-free pressure acid leaching was established to effectively decompose and dissolve the quartz, and remove gangue minerals and fluid inclusions. The calcination process not only removed volatile components; it also destroyed the crystal structure of gangue minerals and enhanced their release probabilities. The calcination process has a positive influence on the removal of impurity elements by the fluoride-free pressure acid leaching process. A total of 85.2 wt % and 84.0 wt % of impurity elements was removed using the leaching systems of HCl-NH_4Cl and H_2SO_4-NH_4Cl, respectively.

Keywords: hydrothermal quartz; geological setting; mineralogy; processing technology

1. Introduction

SiO_2 minerals and rocks play an important role in geological processes and industrial applications [1]. Quartz is one of the most important silica minerals, and it is abundant in the Earth's crust in igneous, metamorphic, and sedimentary rocks [1]. SiO_2 minerals and rocks have been formed by primary and secondary magmatic, hydrothermal, or sedimentary processes or during diagenesis and metamorphosis [2].

Hydrothermal quartz is an important substitute of crystal quartz that has been studied in detail because it is rich in SiO_2 [3,4]. The hydrothermal quartz commonly contains a significant amount of associated minerals and fluid inclusions, which leads to difficulties in quartz processing [5]. Some primary and fine-grained mineral inclusions including mica, feldspar, and hematite are difficult to be removed because they are closely included within quartz grains. Unlike metal ores, the quartz can't be freely ground to cause the decomposition of quartz and fine-grained gangue minerals, because there is a special demand for particle size in quartz sand production [6]. Further, some micron-size fluid inclusions are widely distributed in hydrothermal quartz. Although decrepitation methods at low and medium temperatures (below 700 °C) can enhance the removal of volatile materials in quartz fluid inclusions, the micron-size fluid inclusions rarely are removed, especially in high-temperature quartz [7,8].

Quartz processing technologies have been studied in detail, but systemic research on geological occurrence and mineralogy, combined with optimized processing technologies, is warranted [9,10]. The research on the geological formation and mineralogy of hydrothermal quartz provides an important basis for quartz processing, and helps to characterize the quartz ore and its value.

Processing technologies of high-grade quartz mainly include pre-processing, physical processing (magnetic separation and flotation), chemical treatment (acid leaching and hot chlorination), and thermal treatment (calcination) [11–14]. Furthermore, physical processing and chemical leaching are common processing technologies used in industry. Magnetic separation is mainly used for removing iron-bearing magnetic minerals, while flotation is mainly used for removing aluminum-bearing silicate minerals from quartz ore [15]. However, a common weakness of both processes is that they can only remove specific kinds of impurity minerals. This weakness unavoidably leads to a long process flow during the effective purification of quartz. Although the acid leaching process can effectively remove different impurities at the same time, its leaching solution commonly contains HF, NaF, or CaF. Fluoric reagents, especially hydrofluoric acid, can cause environment pollution [16,17]. Leaching techniques are more effective than flotation for removing intergrown impurities of quartz and gangue minerals [18,19], but the selectivity of acid leaching with hydrofluoric acid is typically low, and this process could sharply reduce particle size of quartz sand as it removed impurities as a result [20,21].

The calcination process, as a thermal treatment technology, is commonly used to reduce reaction time and agent consumption by increasing the exposure probability of gangue minerals and destroying their crystal structures [10,11]. In addition, pressure acid leaching with mixed agents consisting of acids and inorganic salts is deemed to be an effective method to dissolve and remove muscovite without using any fluorides [22]. The metallic ions in the inorganic salts are unacceptable in quartz purification because they would unavoidably drag in metallic impurities during processing, but the use of NH_4Cl avoids the problem. Therefore, leaching systems including HCl-NH_4Cl and H_2SO_4-NH_4Cl could be introduced into quartz purification alongside the calcination process to effectively remove impurities from quartz.

This study presents an analysis of the regional geological setting and mineralogy of the hydrothermal quartz from Hengche Town in the Qichun County of the Hubei Province of China, and further develops a suitable process flow for the purification of hydrothermal quartz. In particular, the research is focused on analyzing occurrences and distributions of impurity elements in the quartz. Based on those results of this mineralogy, a combination process consisting of calcination and fluoride-free acid leaching was developed to remove impurities in the hydrothermal quartz. More importantly, the effects of the calcination and pressure acid leaching on quartz sand were evaluated.

2. Materials and Methods

2.1. Materials and Geological Situation

Quartz ore samples studied are from a hydrothermal vein deposit in Hengche Town in the Qichun County of the Hubei Province in China. The hydrothermal vein deposits are located in the south of a fold belt along the Qinling and Dabie mountains, and close to the Yangtze block. Figure 1 shows a sketch of the geology of the southeast of Hubei Province, China. The Qichun County belongs to the fold belt along the Qinling and Dabie mountains (I), which are bordered by the Yangtze block along the Zengjiaba–Qingfeng–Xiangguang (ZQX) fault zone [23,24]. The reentry belt of high pressure and ultrahigh pressure metamorphism from Tongbai to Dabie (I23) [23,24] was formed by the subduction and collision of the area from late Paleozoic to Triassic, and ended in late Triassic and early Jurassic age. In general, the quartz deposits in the area were formed in the combined belt of Shangdan, influenced by the orogenesis of the Qinling Mountains, and activated by the Yangtze block [23].

Subduction and collision from Paleozoic to Jurassic age caused ore-forming conditions, and the high pressure and ultrahigh pressure rarely contribute to the deposit. As a result, the agglutinated

fine-grained quartz likely contains secondary mineral inclusions in assemblages. In late Triassic to Mesozoic age, the northward subduction and reentry of the Yangtze block or Shangdan Ocean resulted in an orogenic belt south of the Qinling Mountains. This indicates that the geological environment provides a good framework for the deposit formation. Since the quartz deposit is close to the block in the south of the Qinling Mountains, some wall rocks rich in Si, Fe, P, S, and Ca unavoidably have an influence on assemblages of quartz and enlarged sides.

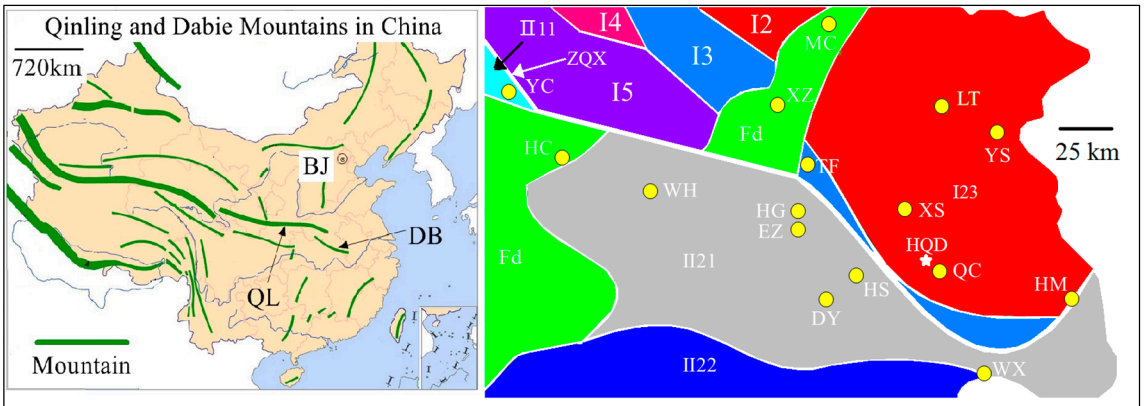

Table of unit classification of geological formations in Hubei Province, China

Grade 1	I				II		
Grade 2	I2 (T)	I3 (Nh-Mz)	I4 (T)	I5 (T)	II1 BDLY (Nh-T_2)	II2	
Grade 3	I23				II11	II21	II22

Figure 1. Locations of the Qinling and Dabie Mountains, and a sketch map of geological formations in the southeast of the Hubei Province in China (Revised according to Mao et al., 2014) [23]: QL—Qinling Mountain, DB—Dabie Mountain, BJ—Beijing, HQD—the hydrothermal quartz deposit, MC—Macheng, YC—Yingcheng, XZ—Xinzhou, LT—Luotian, HC—Hanchuan, TF—Tuanfeng, YS—Yingshan, WH—Wuhan, HG—Huanggang, EZ—Ezhou, XS—Xishui, HS—Huangshi, QC—Qichun, HM—Huangmei, DY—Daye, WX—Wuxue; Fd—Fault depressions, I—Qinling and Dabie fold belt, II—Yangtze block, I2-Combining belt of Shangdan, I3—Block in the southern of Qinling Mountains, I4—Arc basin system from Maota to Suizhou, I5—Combining belt from Liangzhu to Suinan, I23—Reentry belt of high pressure and ultrahigh pressure metamorphism from Tongbai to Dabie, II11—Passive margin in the north rim of Yangzi block, II21—Forelandbasin in the south rim of Yangzi block, II22—Passive margin in the south rim of Yangzi block.

When compared with the few ultrahigh purity quartz deposits (c(Al) < 20 $\mu g \cdot g^{-1}$) in Qichun County [24], the Hengche quartz is from a typical, low-grade and small-scale deposit. In the Luliang age, a hydrothermal solution rich in SiO_2 was split from granite magma. Along the bedding, the vein quartz was formed when the hydrothermal solution invaded into biotite-plagioclase gneiss, granitic gneiss, and amphibolite in the Hongan Group of the Dabie Mountains. The deposit length ranges from 80 m to 115 m, the deposit width ranges from 60 m to 120 m, and the deposit thickness ranges from 5 m to 18 m. The ore mainly contains quartz, and the size of the quartz grain is about 0.8 mm, while a part of the quartz grain is larger than 1 mm.

2.2. Mineralogical Analysis

Examples of the typical bulk hydrothermal quartz were sliced up and polished into sections for microscopy observation. Mineral phases and their distribution in quartz ore were determined by polarizing microscope (DLMP, Leica Microsystems, Wetzlar, Germany). Element components of gangue

minerals were analyzed by electron probe microanalysis (EPMA, JXA-8230, JEOL Ltd., Tokyo, Japan) and X-ray energy spectrometer (EDS).

The electron optical system of EPMA consists of a LaB6 electron gun with a centered cartridge filament; acceleration voltage: 0~30 kV; beam ranging: 10^{-5}~10^{-12} A; and image magnification: ×40~×300,000. Analysis precision of EDS: analysis element: 5B-92U, 2%~3% for common element, detection limit: 0.1 wt %~0.5 wt %. Electron images were obtained at an acceleration voltage of 20.0 kV and a working distance of 11.2 mm. The GBT15617-2002 standard is used for EPMA [25].

2.3. Chemical Analysis

The chemical composition of the hydrothermal quartz was analyzed by inductively coupled plasma (ICP) techniques according to national standards SJ/T 11554-2015 [26] and GB/T 32650-2016 [27] in China. The analytical method and procedure are as follows.

2.0000 g per sample were dissolved by 12 cm^3 hydrofluoric acid (40 wt %, guarantee reagent) in a pressure-tight reaction kettle with a lining of polytetrafluoretyhylene (PTFE, 50 cm^3), while digestion temperature and time were 200 °C and 3 h, respectively. The produced fluid was heated and evaporated in a PTFE beaker at 150 °C. When the fluid shrank into droplets, 3 cm^3 ultrapure water was added for further evaporation, while the operation was repeated three times, and the remained fluid was commonly diluted to 20 cm^3, 500 cm^3, or 1000 cm^3, according to the different contents of impurity elements.

The element contents of diluted fluids were analyzed by inductively coupled plasma-optical emission spectroscopy (ICP-OES, Prodigy 7, LEEMAN LABS INC., Hudson, NH, USA) and inductively coupled plasma mass spectrometry (ICP-MS, iCAP-Qc, THERMO FISHER SCIENTIFIC, Waltham, MA, USA).

The analytical conditions include:

Wavelength coverage of ICP-OES: 165~1100 nm, optical resolution: 0.007 nm at 200 nm, relative standard deviation: <2%.

Mass spectrum of ICP-MS: 4~290 amu, sensitivity: >150 Mcps·ppm^{-1} for common elements, detection limit: <0.1 ppt for common element, relative standard deviation: <2% in short time, <3% in long time.

The computational formula to obtain the element contents is as follows:

$$\varphi = \frac{V(\rho - \rho_0)}{m} \quad (1)$$

where φ is the mass of element content in 1 g of quartz sand, μg·g^{-1}; V is the volume of the diluted fluid, cm^3; ρ is the mass concentration of the ananlyzed element by ICP, ρ_0 is the mass concentration of the blank sample, mg·dm^{-3} or μg·dm^{-3}; m is the mass of the analyzed sample, 2.0000 g.

2.4. Processing and Characterization of Quartz Sand

Mining, washing, crushing, and grinding of quartz ore were accomplished by Kaidi Building Materials Co., Ltd. (Huangshi, China). The mined quartz ore was washed and air-dried. Then, the bulk quartz was crushed by a jaw crusher (PE-Φ100 × 125), and ground by a Raymond mill (3R2115). Produced quartz sand ranging from 106 μm (140 mesh) to 212 μm (70 mesh) was selected by standard sieve, and used for experiments. The quartz sand was calcinated at 900 °C for 5 h in a muffle furnace (KSY-12-16A), and then cooled by ultrapure water (18.2 MΩ·cm). The calcinated quartz sand was leached by mixed leaching agents in a pressure-tight reaction kettle. Leached quartz sand was washed by ultrapure water, and the leach liquor and washing liquor were mixed to wash the calcinated quartz sand in turn. Quartz and gangue minerals during processing were observed by scanning electron microscope (SEM, JSM-IT300) and EPMA after carbon coating.

Secondary electron images were obtained at 20.0 kV of acceleration voltage, 16.2~16.6 mm of working distance, and 30 nm of spot size.

3. Results and Discussion

3.1. Mineralogy of Hydrothermal Quartz

Bulk quartz is milky-white as a whole, and its size ranges from 20 cm to 40 cm. Scattered red materials are distributed in quartz fractures.

3.1.1. Impurity Elements in Quartz Ore

Elemental concentrations of the quartz sand are shown in Table 1. The main impurity elements determined by ICP are Al (353 $\mu g \cdot g^{-1}$), K (118 $\mu g \cdot g^{-1}$), Fe (61.2 $\mu g \cdot g^{-1}$), P (15.5 $\mu g \cdot g^{-1}$), Na (13.4 $\mu g \cdot g^{-1}$), Mg (11.8 $\mu g \cdot g^{-1}$), B (10.8 $\mu g \cdot g^{-1}$), Ti (8.31 $\mu g \cdot g^{-1}$) and Ca (8.04 $\mu g \cdot g^{-1}$) by ICP analysis, and proportions of these elements in total impurities are 57.0 wt %, 19.1 wt %, 9.89 wt %, 2.50 wt %, 2.16 wt %, 1.91 wt %, 1.74 wt %, 1.34 wt % and 1.30 wt %, respectively.

Table 1. Contents of main impurity elements within the hydrothermal quartz analyzed by inductively coupled plasma (ICP) analysis.

Element	**Al**	**Fe**	**Na**	**S**	**P**	**Li**	**K**	**Ca**	**Ti**
Content [1] ($\mu g \cdot g^{-1}$)	353	61.2	13.4	5.64	15.5	2.20	118	8.04	8.31
Element	**Mg**	**Ni**	**Zr**	**Zn**	**As**	**B**	**In Total**		
Content ($\mu g \cdot g^{-1}$)	11.8	1.01	6.46	0.567	3.16	10.8	619		

[1] Relative standard deviations (RSD) are less than 4%.

3.1.2. Optical Microscope Analysis

The hydrothermal quartz mainly contains solid inclusions of muscovite and hematite, as well as fluid inclusions (Figure 2). The muscovite platelets are widely distributed along the quartz grain boundaries (Figure 2a), but a small quantity of muscovite is included in the quartz grains (Figure 2b). Muscovite is commonly thought to be an important source of impurity elements, including Al, K, Mg, Fe and Ti [28].

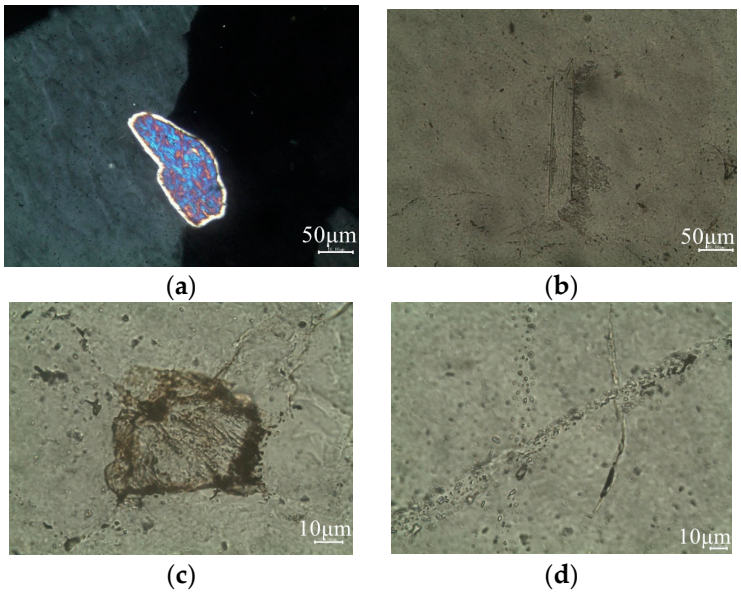

Figure 2. Transmitted-light microscopy images of muscovite, hematite, and fluid inclusions within quartz thin sections: (**a**) muscovite along a grain boundary (XPL); (**b**) muscovite included in quartz crystal (PPL); (**c**) hematite in compression fractures of quartz (PPL); (**d**) two generations of fluid inclusions (PPL).

Hematite is the main iron carrier in these veins, and mainly occurs filling thin cracks (Figure 2c). In hydrothermal quartz, most of the fluid inclusion generations (Figure 2d) traverse the whole quartz grains, so these secondary fluid inclusions commonly containing gas and liquid phases are a possible source of fluid impurities [29].

3.1.3. Electron Probe Microanalysis

Figure 3 shows secondary electron images of muscovite, hematite, apatite, and quartz sections. Figure 3a is a micrograph of muscovite inclusions within quartz. The analysis (Table 2) shows that Al, K, Mg, and Fe are the major elements obtained in the muscovite. These impurities occurring in aluminum silicate minerals could reduce the quality of quartz production [30]. Figure 3b is an image of hematite (the mineral phase was determined by polarizing microscope within an electron probe microanalyzer) in quartz, and its composition (Table 2) shows that the secondary mineral contains elevated Fe (the Cr is from polishing powder). Generally, the iron in high-grade quartz is typically less than 1 ppm [31]. It is difficult to remove some filmy iron on the surface of quartz particles by conventional physical methods [32]. Figure 3c is an image of apatite, which is associated with hematite. Its chemical analysis (Table 2) shows that P, Ca, Fe, Mg, and Na occur in the mixed minerals. The apatite is included in quartz, and it is a diagnostic mineral of hydrothermal quartz [33].

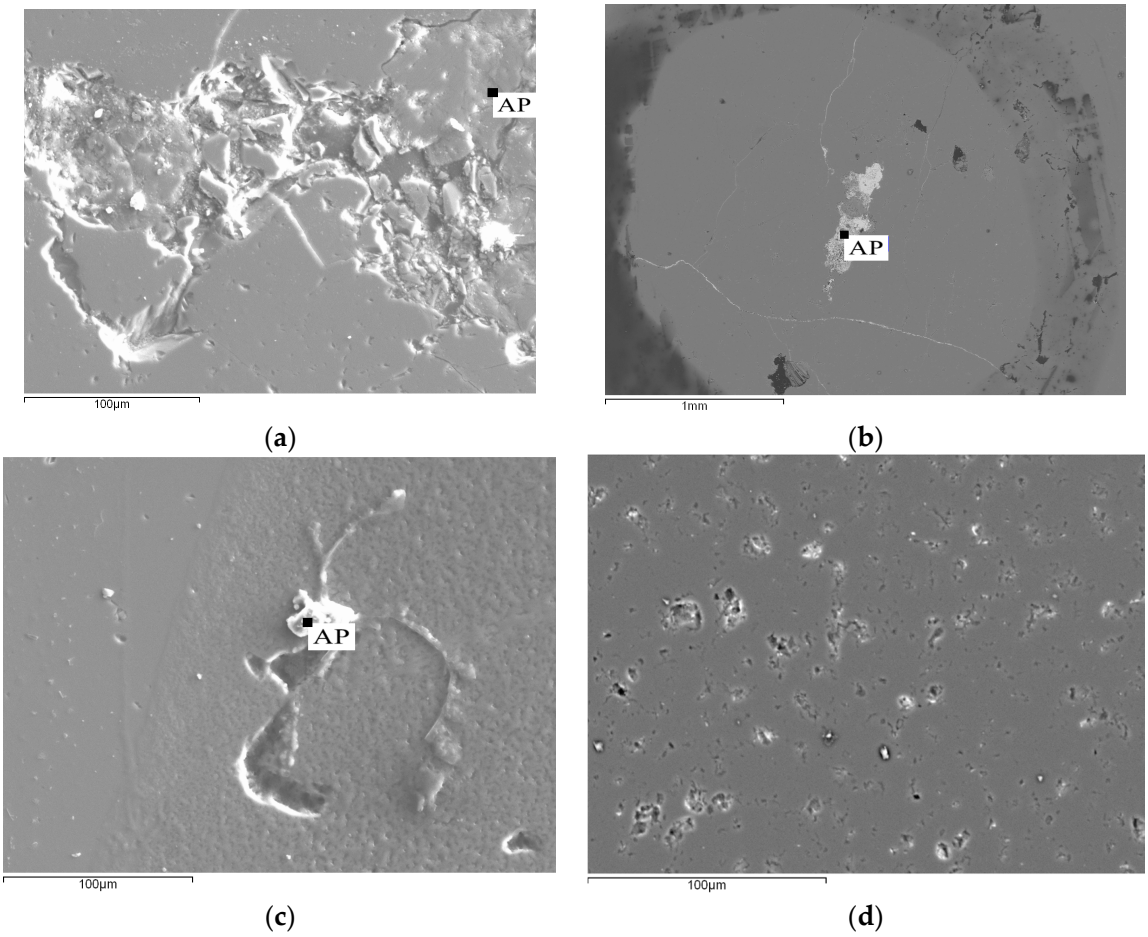

Figure 3. Details of solid inclusions in quartz veins using EMP (electron microprobe) images in SE (secondary electron) mode: (**a**) muscovite inclusions in quartz; (**b**) hematite in quartz fracture; (**c**) apatite and hematite included in quartz; (**d**) a typical microarea used for area-scan analysis of the electron probe; AP—analyzed point by X-ray energy spectrometer (EDS).

Table 2. Elemental components of analyzed points in Figure 3a–c by EDS analysis of electron probe.

Element	Na	Mg	Al	Si	P	S	K	Ca	Mn	Cr	Fe	O
Figure 3a (wt %)		0.31	19.16	24.69			8.40				0.28	47.17
RSD [1] (%)		2.43	1.10	0.96			1.22				1.96	
Figure 3b (wt %)			2.24	2.48	0.63					2.89	65.91	25.85
RSD (%)			2.23	1.32	2.64					1.08	0.68	
Figure 3c (wt %)	3.31	5.06	1.57	6.63	10.38	2.01	0.87	14.50	0.91		14.52	40.24
RSD (%)	2.88	2.09	2.11	1.16	1.67	1.34	2.89	1.44	1.57		0.83	

[1] Relative standard deviations (RSD) are less than 3%.

Besides impurities in these inclusions of the quartz, some lattice elements in the hydrothermal quartz cannot be neglected. As shown in Figure 4, Götze (2009) [34] reported four substitutions between Si and impurity elements in a quartz lattice. In addition, substitution with interstitial charge compensator is suitable to be used for explaining occurrences of impurity elements in the hydrothermal quartz, because P mainly occurs in the apatite, and Ge is not detected by ICP analysis.

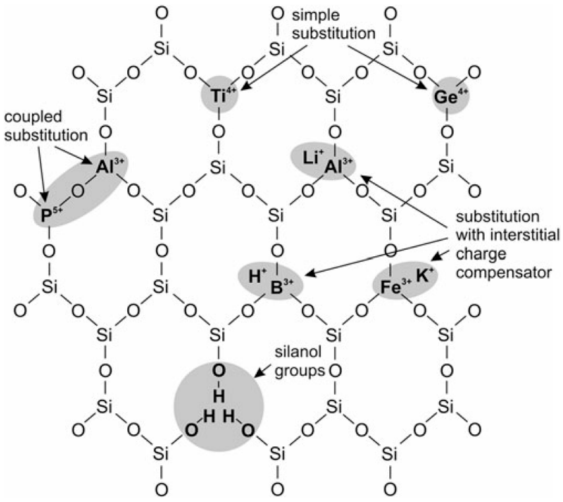

Figure 4. Schematic quartz structure showing the configuration of trace elements in the quartz lattice (modified from Götze 2009) [34]. Mclaren et al. (1983) proposed that the substitution of Si^{4+} by four H^+ is also possible (silanol groups) [35]. Since the illustration is two-dimensional, the fourth H^+ is not shown on the figure.

Figure 5 shows the surface distributions of Si, O, Al, and Na in the microarea of Figure 3d. Al and Na are uniformly distributed across the microarea. This indicates that the two elements replace Si in a quartz lattice in substitution with the interstitial charge compensator, although Li and B cannot be effectively detected by electron probe.

Based on a combination of optical microscope analysis and electronic microscope analysis, the main mineral inclusions in the quartz are muscovite, hematite and apatite. The muscovite contains Al, K, Mg, and Fe. The hematite contains Fe, while some hematite is associated with apatite. The apatite contains P and Ca. The associated Na, Mg, and Al might be from the wall rock of biotite plagioclase gneiss. For the main impurities Al, K, and Fe, the microscopic examination and component analysis indicate that Al and K mainly occur in muscovite, and Fe mainly exists in hematite. In addition, some Al and Na possibly occur in the quartz lattice. In addition, fluid inclusions can be possible sources for H, Na, and othe alkali and alkali Earth elements (and probably anions such as Cl). Most of the fluid inclusions contain gas and liquid phases, and are secondary. The quartz ore mainly contains quartz, muscovite, hematite, apatite, and secondary fluid inclusions, which are common features of hydrothermal deposits [36].

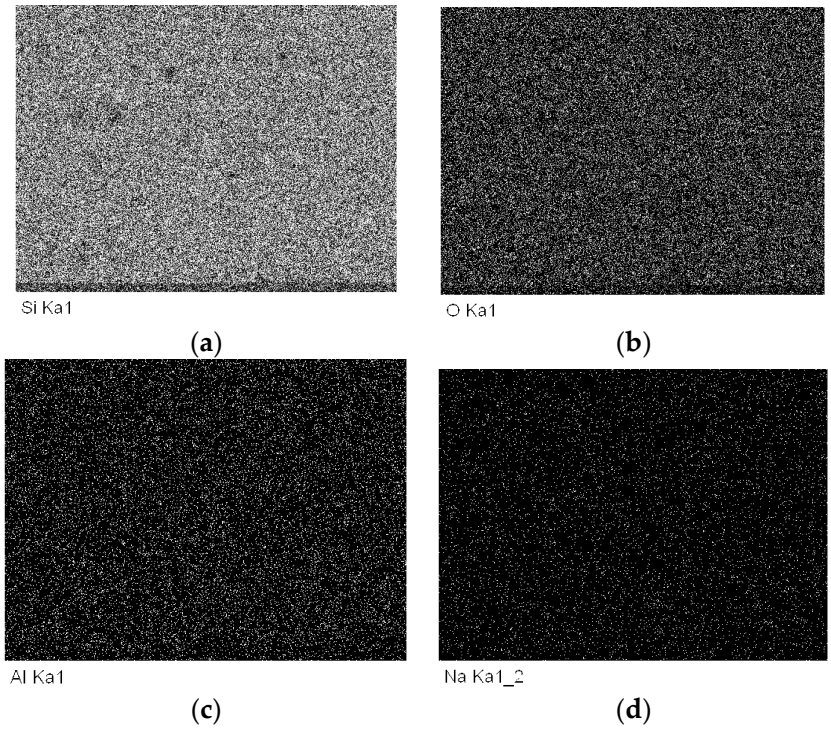

Figure 5. Surface distributions of Si, O, Al, and Na in the microarea of Figure 3d (analyzing for 12 min): luminance was enhanced for showing clearly: (**a**) the surface distribution of Si; (**b**) the surface distributions of O; (**c**) the surface distribution of Al; and (**d**) the surface distributions of Na. White spots represent elements at the corresponding positions of Figure 3d, and the scale bars are the same as Figure 3d.

3.2. Quartz Processing

Xiong et al. used pressure acid leaching with hydrofluoric acid as an efficient purification process for purifying the vein quartz [10]. However, in the conventional acid leaching process of quartz ore, quartz purification depends on an acid attack to gangue minerals, which results in high acid consumption and a long leaching time [10,11,22]. The two problems significantly reduce equipment life, increase production costs, and decrease production efficiency. Due to the pollution of the fluoric leaching agent [16,17], it is therefore necessary to develop an efficient fluorine-free leaching system to purify vein quartz. The objective of the recommended process is to realize a fluoride-free technology of pressure acid leaching at the same time as ascertaining quartz quality.

Calcination at 900 °C for 5 h is deemed to be effective to remove organic impurities and H_2O within fluid inclusions, and increase the exposure probabilities of mineral inclusions, including muscovite, hematite, and apatite, according to different thermal expansibilities [10,11,37]. In addition, calcination could destroy the crystal structures of gangue minerals, especially muscovite [37]. When combined with the calcination process, pressure acid leaching has the power to effectively purify quartz sand without any fluorides.

3.2.1. Recommended Process

Figure 6 shows two recommended processes for purifying the hydrothermal quartz. Quartz sand was calcinated at 900 °C for 5 h, and the calcinated quartz sand was washed by leaching and washing liquors. In a pressure-tight reaction kettle [10], the washed quartz sand was either leached by acid solutions containing H_2SO_4 and NH_4Cl, or HCl and NH_4Cl. Leached quartz sand was again washed by ultrapure water 5–10 times, and then dried at 105 °C for 3 h.

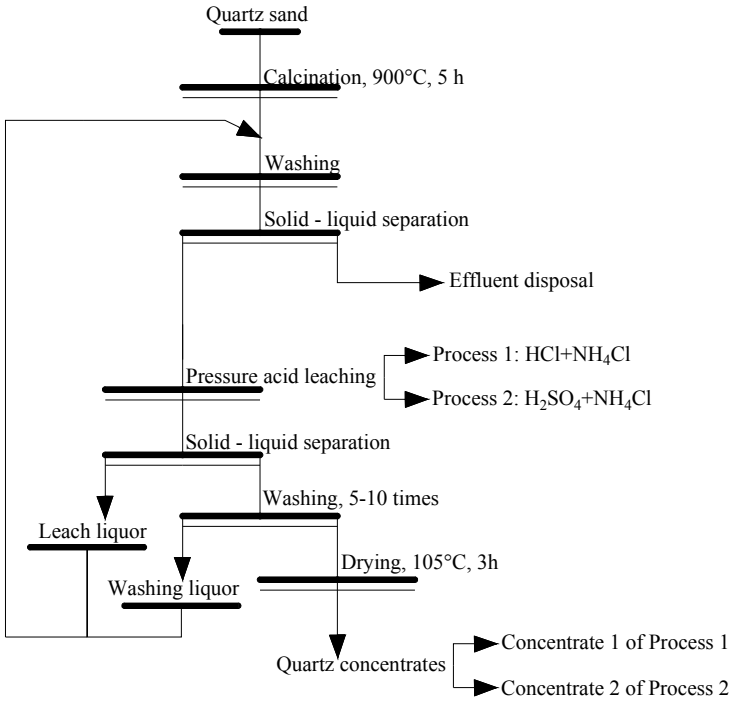

Figure 6. Engineering flow sheet of the recommended processes for purifying the hydrothermal quartz.

Following calcination, the first washing process is used to make full use of acids remained in leaching and washing liquors, and cut the cost effluent disposal. Using H_2SO_4 or HCl, calcinated gangue minerals can be efficiently dissolved and removed from quartz at high pressure and temperature. The NH_4Cl is used to provide hydrogen ions with a more stable and higher concentration during the hydrolysis of NH_4^+.

Based on a combination of calcination and pressure acid leaching, the quartz sand was efficiently purified. The optimal process conditions and contents of impurity elements in quartz concentrates for two leaching processes are shown in Tables 3 and 4, respectively. The effective removal of Al, K, and Fe indicates that the main gangue minerals, including muscovite and hematite, are efficiently removed by the two processes. Parts of P and Ca were removed, but the removal rates were not so high. The possible reason is that some primary apatite is included in the quartz particle, and some P occurs in the quartz lattice. S, Ni, Zn, and As are not detected in quartz concentrates, which indicates that these impurity elements are liberated from quartz particles after ore grinding. Zr occurs in hydrothermal zircon due to the ultra-high pressure action in the Dabie Mountains [38], but it is difficult to be dissolved by acid solution [39], so its removal rates are only 0.155 wt %. The removal rates of some elements, including Li, B, Na, P, and Ti, are not so high because parts of them occur in the quartz lattice. As a result, the fluoride-free leaching processes have little influence on removing them.

Table 3. Optimal conditions of leaching processes 1 and 2.

Leaching Process	Temperature (°C)	Acid Concentration (HCl or H_2SO_4) ($mol \cdot dm^{-3}$)	NH_4Cl Concentration ($mol \cdot dm^{-3}$)	Liquid/Solid Ratio ($cm^3 \cdot g^{-1}$)	Leaching Time (h)
HCl + NH_4Cl	280	0.8	0.8	10	6
H_2SO_4 + NH_4Cl	250	0.3	0.45	5	7

Table 4. Contents and removal rates of major elements at optimal conditions in Table 3.

Element	Ore (μg·g^{-1})	Concentrate 1 [1] (μg·g^{-1})	Removal Rate 1 (wt %)	Concentrate 2 [1] (μg·g^{-1})	Removal Rate 2 (wt %)
Al	353	41.5	88.2	44.1	87.5
Fe	61.2	1.14	98.1	1.12	98.2
Na	13.4	11.3	15.7	12.2	8.96
S	5.64	-	-	-	-
P	15.5	5.00	67.7	5.39	65.2
Li	2.20	2.19	0.455	2.04	7.27
K	118	1.21	99.0	2.24	98.1
Ca	8.04	4.54	43.5	4.40	45.3
Ti	8.31	4.89	41.2	5.38	35.3
Mg	11.8	4.88	58.6	7.15	39.4
Ni	1.01	-	-	-	-
Zr	6.46	6.45	0.155	6.45	0.155
Zn	0.567	-	-	-	-
As	3.16	-	-	-	-
B	10.8	8.77	18.8	8.77	18. 8
In total	619	91.9	85.2	99.2	84.0

[1] Relative standard deviations (RSD) of element contents in quartz concentrates are less than 4%, and not shown in the Table; (-) = below the limit of detection.

3.2.2. Effects of the Calcination Process

Muscovite, as a main gangue mineral in the hydrothermal quartz, can be transformed into amorphous phases during the calcination process [37]. Figure 7 shows the surface topographies of muscovite in calcinated quartz sand. The planar water and constitution water were removed from the muscovite during calcination (Formula (2)), and the water evaporation increased the interlayer spacing of the muscovite [37], and further promoted a seperation of different muscovite sheets along the cleavage plane (Figure 7a). Muscovite flakes close to its surface were separated from the host, and some of them were damaged into fragments with micron sizes (Figure 7b). The fragments consisting of active K_2O, Al_2O_3, and SiO_2 (Formula (3)) could be easily dissolved by acid solutions. This demonstrates that calcination is a necessary procedure for removing muscovite by a fluoride-free acid leaching process.

$$K_2O{\cdot}3Al_2O_3{\cdot}6SiO_2{\cdot}2H_2O = K_2O{\cdot}3Al_2O_3{\cdot}6SiO_2 + 2H_2O\uparrow \quad (2)$$

$$K_2O{\cdot}3Al_2O_3{\cdot}6SiO_2 = K_2O + 3Al_2O_3 + 6SiO_2 \quad (3)$$

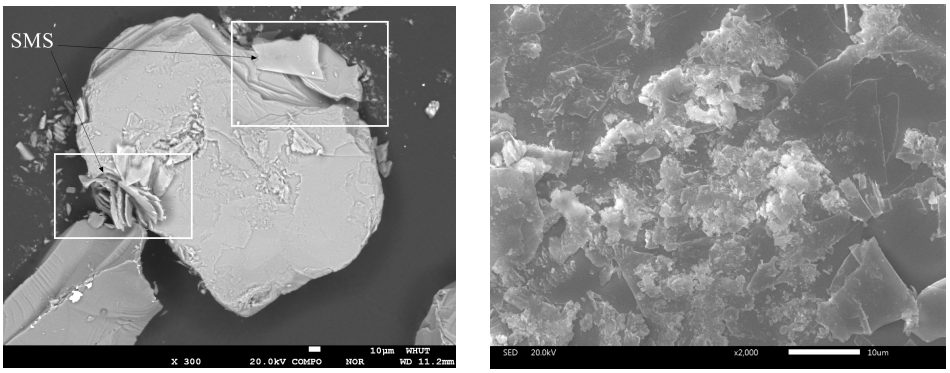

(**a**) (**b**)

Figure 7. Surface topographies of muscovite in calcinated quartz sand: calcination temperature 900 °C, calcination time 5 h; (**a**) backscattered electron image obtained by electron probe microanalysis (EPMA); (**b**) secondary electron image obtained by scanning electron microscope (SEM); SMS—seperated muscovite sheets along cleavage plane.

The calcination process is also effective for removing other mineral inclusions, such as hematite and apatite. The exposure probabilities of gangue minerals included in quartz grains have great influences on impurities removal. The impurities included in quartz particles are hardly removed unless a calcination process is used, especially in case of a fluoride-free purification process of quartz sand. The different expansion coefficients between quartz and hematite during calcination promoted the exposure of hematite. The calcination is also effective for apatite when it is associated with hematite.

Calcination is also an effective method for removing fluid impurities within quartz fluid inclusions. Schmidt–Mumm [40] thought that the decrepitation of the fluid inclusions could be classified as several processes: microcracks opening and propagating, the rupture of grain boundaries, transgranular fracturing, intragranular fracturing, and the decrepitation of large/small fluid inclusions. Figure 8 shows a decrepitation pit on the surface of a calcinated quartz particle. The small pit is about 7 μm long and 1μm wide. It indicates that calcination at 900 °C for 5 h can even remove micron-size fluid inclusions. Volatile materials occurring in the fluid inclusions were removed during the calcination process, and inorganic salts dissolved in the fluids could be leached in the following acid leaching process.

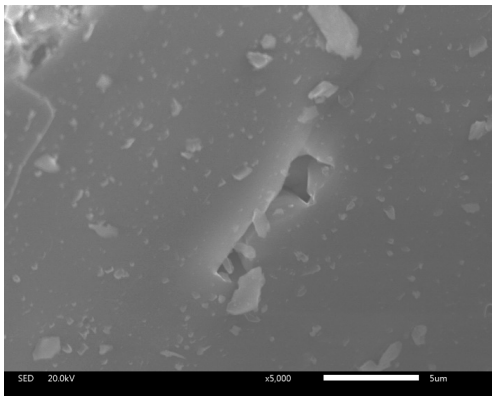

Figure 8. Decrepitation pit on the surface of a calcinated quartz particle: calcination temperature 900 °C, calcination time 5 h.

At the optimal leaching conditions of processes 1 and 2 in Table 3, the element contents in quartz sand only after pressure acid leaching (rather than using a calcination process) were compared with those of quartz concentrates so as to describe the effect of the calcination process on the removal of impurity elements. As shown in Table 5, the calcination process can effectively promote the leaching of Al, Fe, S, P, K, and As. The contents of Al and K were respectively reduced from 167 and 188 $\mu g \cdot g^{-1}$ to 41.5 and 44.1 $\mu g \cdot g^{-1}$ by an additional calcination process. The differences indicate that the calcination process activates some gangue minerals and reduces the chemical reaction resistance of the leaching process by destroying their crystal structures. In addition, the decrease of the Fe and P contents may be caused by exposure of the hematite and apatite during calcination. S and As could easily be removed during calcination due to their volatility. Moreover, the decrease of Ca and Na contents might be caused by the decrepitation of fluid inclusions (compare to Figure 8).

Table 5. Contents of major elements in quartz sand with or without a calcination process.

Element	Ore ($\mu g \cdot g^{-1}$)	C and PHAL ($\mu g \cdot g^{-1}$)	PHAL [1] ($\mu g \cdot g^{-1}$)	C and PSAL ($\mu g \cdot g^{-1}$)	PSAL [1] ($\mu g \cdot g^{-1}$)
Al	353	41.5	167	44.1	188
Fe	61.2	1.14	7.42	1.12	13.4
Na	13.4	11.3	13.5	12.2	12.9
S	5.64	-	4.00	-	4.52
P	15.5	5.00	13.6	5.39	10.4
Li	2.20	2.19	2.20	2.04	2.19

Table 5. *Cont.*

Element	Ore (μg·g^{-1})	C and PHAL (μg·g^{-1})	PHAL [1] (μg·g^{-1})	C and PSAL (μg·g^{-1})	PSAL [1] (μg·g^{-1})
K	118	1.21	42.6	2.24	45.9
Ca	8.04	4.54	7.50	4.40	8.01
Ti	8.31	4.89	6.07	5.38	5.91
Mg	11.8	4.88	8.60	7.15	8.12
Ni	1.01	-	-	-	-
Zr	6.46	6.45	6.46	6.45	6.46
Zn	0.567	-	-	-	-
As	3.16	-	1.47	-	2.15
B	10.8	8.77	9.80	8.77	8.47
In total	619	91.9	290	99.2	316

[1] Relative standard deviations (RSD) of the element contents in quartz concentrates are less than 4%, and not shown in the Table; C—calcination process (900 °C for 5 h), PHAL—pressure acid leaching (HCl + NH_4Cl), PSAL—pressure acid leaching (H_2SO_4 + NH_4Cl); (-) = below the limit of detection.

3.2.3. Effects of Fluoride-Free Pressure Acid Leaching

Figure 9 shows the surface topographies of muscovite in leached quartz sand. Compared with the surface topographies of muscovite (Figure 7) in calcinated quartz sand, the fragments with micron sizes were dissolved and removed from the muscovite surface (Figure 9a). This process can be described by the dissolution of the active fragments containing K_2O and Al_2O_3 (Formulas (4) and (5)). In addition, the muscovite in calcinated quartz sand was further dissolved along its edge. More importantly, some fractures were developed in the vertical direction of the long side of muscovite when concentrations of leaching agents were doubled (Figure 9b). Moreover, expanded interlayer spacing provided favorable conditions for leaching reactions, and promoted a faster process of muscovite dissolution. The several effects of acid leaching led to the structure collapsing and the dissolution of muscovite.

$$K_2O + 2H^+ = 2K^+ + H_2O \quad (4)$$

$$Al_2O_3 + 6H^+ = 2Al^{3+} + 3H_2O \quad (5)$$

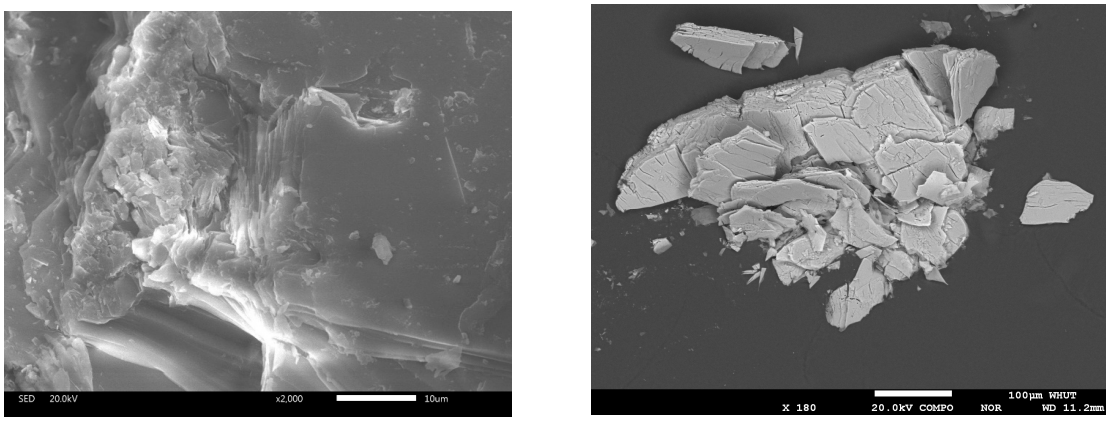

(**a**) (**b**)

Figure 9. Surface topographies of muscovite in leached quartz sand: (**a**) secondary electron image obtained by SEM, leaching conditions: 0.05 mol·dm^{-3} H_2SO_4, 0.10 mol·dm^{-3} NH_4Cl, liquid/solid ratio 5 cm^3·g^{-1}, leaching time 7 h, and leaching temperature 200 °C; (**b**) backscattered electron image obtained by EPMA, leaching conditions: 0.10 mol·dm^{-3} H_2SO_4, 0.20 mol·dm^{-3} NH_4Cl, liquid/solid ratio 5 cm^3·g^{-1}, leaching time 7 h, and leaching temperature 200 °C.

During calcination, most of the mineral inclusions in quartz sand were transformed into mineral intergrowths of quartz and gangue minerals due to heat stress. Then they were exposed in the

leaching solution. With further calcination, the mineral intergrowth was promoted into separated mineral monomers. Figure 10 shows the surface topographies of calcinated and leached quartz sands. Although associated minerals were liberated from quartz particles in Figure 10a, some impurities unavoidably remained in the pores of the calcinated quartz surface. The impurities that remained on the surface of calcinated quartz were leached by mixed leaching agents. As a result, the surface of the leached quartz sand in Figure 10b became smoother than that of the calcinated quartz sand in Figure 10a. Common intergrowths of quartz–hematite and quartz–hematite–apatite were leached by mixed leaching agents, and the leaching processes are as follows:

$$Fe_2O_3 + 6H^+ = 2Fe^{3+} + 3H_2O \quad (6)$$

$$Ca_5[PO_4]_3(OH) + H^+ \rightarrow Ca^{2+} + H_3PO_4 + H_2PO_4^- + HPO_4^{2-} + PO_4^{3-} + H_2O \quad (7)$$

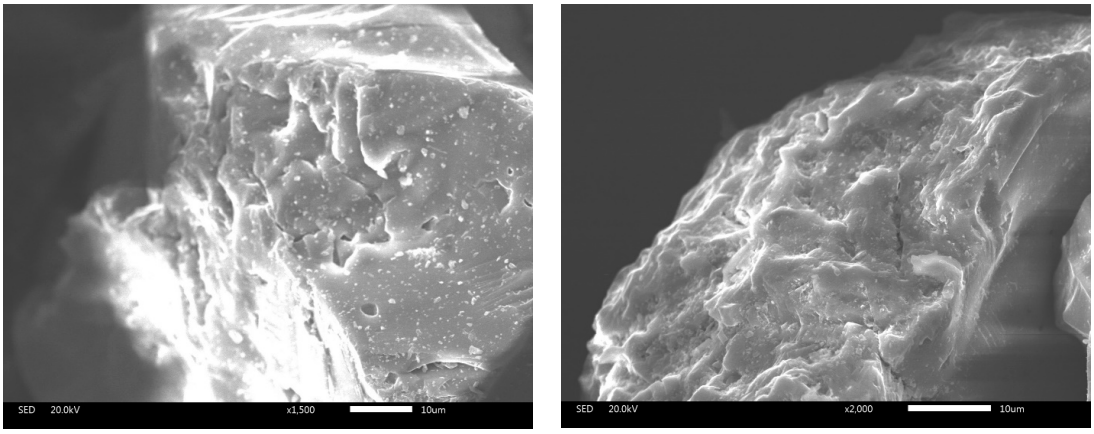

(**a**) (**b**)

Figure 10. Surface topographies of quartz sand: (**a**) calcinated quartz sand (900 °C for 5 h); (**b**) quartz concentrate of process 2.

By a combined process of calcination and fluoride-free acid leaching, gangue minerals including muscovite, hematite, and apatite were effectively separated from the hydrothermal quartz. The calcination process not only destroyed the crystal structures of the gangue minerals; it also removed volatile compounds. Meanwhile, the exposure probabilities of the impurities were enhanced due to the calcination process. In general, the calcination process had a positive influence on the removal of impurity elements with the fluoride-free pressure acid leaching process.

4. Conclusions

The present study analyzed the geological formation and mineralogy of the hydrothermal quartz deposit from Hengche in Qichun County, of the Hubei Province in China, A combined purification process consisting of calcination and fluoride-free pressure acid leaching was developed based on two fundamental investigations. Moreover, the effects of this processing procedure on the raw quartz material were discussed, and the following conclusions obtained:

(1) Impurity elements in the hydrothermal quartz are related to fluid inclusions and associated gangue minerals such as muscovite, hematite, and apatite. The muscovite not only occurs along the grain boundaries of quartz particles; it is also included in quartz particles. The hematite is mainly of secondary origin, and occurs along crystal fractures in quartz. However, some of the hematite is also associated with apatite.

(2) The gangue minerals such as muscovite, hematite, and apatite were effectively removed by a combined process of calcination and fluoride-free pressure acid leaching, while the removal rates

of the most important impurity elements Al, K, and Fe were 88.2 wt %, 99.0 wt % and 98.1 wt %, respectively, for the HCl-NH_4Cl system, and 87.5 wt %, 98.1 wt % and 98.2 wt % for the H_2SO_4-NH_4Cl system. The removal rates of some elements, including Li, B, Na, P and Ti were not so high, because they might be structurally incorporated in the quartz lattice.

(3) The calcination process not only destroyed the crystal structure of the gangue minerals, it also removed volatile compounds. The liberation probabilities of impurities were enhanced due to the calcination process. In conclusion, the calcination process had a positive influence on the removal of impurity elements during the fluoride-free pressure acid leaching process.

Acknowledgments: This research was supported by the Open Foundation of Engineering Center of Avionics Electrical and Information Network of Guizhou Province Colleges and Universities of Anshun University (HKDZ201404).

Author Contributions: Min Lin and Zhneyu Pei conceived and designed the experiments; Min Lin performed the experiments; Min Lin, Zhneyu Pei and Shaomin Lei analyzed the data; Shaomin Lei contributed reagents/materials/analysis tools; Min Lin wrote the paper.

Conflicts of Interest: The authors declare no conflict of interest. The founding sponsors had no role in the design of the study; in the collection, analyses, or interpretation of data; in the writing of the manuscript, and in the decision to publish the results.

References

1. Götze, J. Classification, mineralogy and industrial potential of SiO_2, minerals and rocks. In *Quartz: Deposits, Mineralogy and Analytics*, 1st ed.; Götze, J., Möckel, R., Eds.; Springer: Berlin/Heidelberg, Germany, 2012; pp. 1–27.
2. Howm, R.A. Silica: Physical behavior, geochemistry and materials applications. *Mineral. Mag.* **1996**, *60*, 390–391. [CrossRef]
3. Armington, A.F.; Larkin, J.J. Purification and analysis of α-quartz. *J. Cryst. Growth* **1986**, *75*, 122–125. [CrossRef]
4. Li, J.S.; Li, X.X.; Shen, Q.; Zhang, Z.Z.; Du, F.H. Further purification of industrial quartz by much milder conditions and a harmless method. *Environ. Sci. Technol.* **2010**, *44*, 7673. [CrossRef] [PubMed]
5. Bayaraa, B.; Greg, B.; Noriyoshi, T. Hydrothermal quartz vein formation, revealed by coupled SEM-CL imaging and fluid inclusion microthermometry: Shuteen Complex, South Gobi, Mongolia. *Resour. Geol.* **2010**, *55*, 1–8. [CrossRef]
6. Johnson, G.R. History of the industrial production and technical development of single crystal cultured quartz. In Proceedings of the IEEE International Frequency Control Symposium & Exposition, Montreal, QC, Canada, 23–27 August 2004.
7. Mavrogenes, J.A.; Bodnar, R.J. Hydrogen movement into and out of fluid inclusions in quartz: Experimental evidence and geologic implications. *Geochim. Cosmochim. Acta* **1994**, *58*, 141–148. [CrossRef]
8. Tomlinson, E.L.; Mcmillan, P.F.; Zhang, M.; Jones, A.P.; Redfern, S.A.T. Quartz-bearing C–O–H fluid inclusions diamond: Retracing the pressure–temperature path in the mantle using calibrated high temperature IR spectroscopy. *Geochim. Cosmochim. Acta* **2007**, *71*, 6030–6039. [CrossRef]
9. Sayilgan, A.; Arol, A.I. Effect of carbonate alkalinity on flotation behavior of quartz. *Int. J. Miner. Process.* **2004**, *74*, 233–238. [CrossRef]
10. Xiong, K.; Lei, S.M.; Zhong, L.L.; Pei, Z.Y.; Yang, Y.Y.; Zang, F.F. Thermodynamic mechanismand purification of hot press leaching with vein quartz. *China Min. Mag.* **2016**, *25*, 129–132. [CrossRef]
11. Lei, S.M.; Pei, Z.Y.; Zhong, L.L.; Ma, Q.L.; Huang, D.D.; Yang, Y.Y. Study on the technology and mechanism of reverse flotation and hot pressing leaching with vein quartz. *Nonmet. Mines* **2014**, *37*, 40–43. [CrossRef]
12. Wang, L.; Li, C.X.; Wang, Y.; Yin, D.Q. China technologies present of high-purity quartz processing and the development propositions. *J. Mineral. Petrol.* **2011**, *31*, 110–114. [CrossRef]
13. Haßler, S.; Kempe, U.; Monecke, T.; Götze, J. Trace Element Content of Quartz from the Ehrenfriedersdorf Sn-w Deposit, Germany: Results of an Acid-Wash Procedure. In *Mineral Deposit Research: Meeting the Global Challenge, Proceedings of the Eighth Biennial SGA Meeting, Beijing, China, 18–21 August 2005*; Mao, J.W., Bierlein, F.P., Eds.; Society of Economic Geologists, Inc.: Littleton, CO, USA, 2006.

14. Haus, R.; Prinz, S.; Priess, C. Assessment of high purity quartz resources. In *Quartz: Deposits, Mineralogy and Analytics*, 1st ed.; Götze, J., Möckel, R., Eds.; Springer: Berlin/Heidelberg, Germany, 2012; pp. 45–49.
15. Vidyadhar, A.; Hanumantha, R.K. Adsorption mechanism of mixed cationic/anionic collectors in feldspar-quartz flotation system. *J. Colloid Interface Sci.* **2007**, *306*, 195–204. [CrossRef] [PubMed]
16. An, J.; Lee, H.A.; Lee, J.; Yoon, H.O. Fluorine distribution in soil in the vicinity of an accidental spillage of hydrofluoric acid in Korea. *Chemosphere* **2015**, *119*, 577–582. [CrossRef] [PubMed]
17. Dasgupta, P.K. Comment on "hydrofluoric acid in the Southern California atmosphere". *Environ. Sci. Technol.* **1998**, *31*, 427. [CrossRef]
18. Zhou, Y.H. Study on refining quartz powder by leaching in HF acid solution. *J. Mineral. Petrol.* **2005**, *25*, 23–26. [CrossRef]
19. Scott, H.S. The decrepitation method applied to minerals with fluid inclusions. *Econ. Geol.* **1948**, *43*, 637–654. [CrossRef]
20. Knotter, D.M. Etching mechanism of vitreous silicon dioxide in HF-Based solutions. *J. Am. Chem. Soc.* **2000**, *122*, 4345–4351. [CrossRef]
21. Su, Y.; Zhou, Y.H.; Huang, W.; Gu, Z.A. Study on reaction kinetics between silica glasses and hydrofluoric acid. *J. Chin. Ceram. Soc.* **2004**, *32*, 287–293. [CrossRef]
22. Xue, N.N.; Zhang, Y.M.; Liu, T.; Huang, J.; Zheng, Q.S. Effects of hydration and hardening of calcium sulfate on muscovite dissolution during pressure acid leaching of black shale. *J. Clean Prod.* **2017**, *149*, 989–998. [CrossRef]
23. Mao, X.W.; Ye, Q.; Liao, M.F.; Yang, J.X.; Zhang, H.J.; Wang, Z.Y. Division and discussion of geotectonic units in Hubei Province. *Resour. Environ. Eng.* **2014**, *1*, 6–15. [CrossRef]
24. Zhang, P.C.; Liu, Y.F.; Li, J.F.; Deng, M.; Liu, S.T. Study on high-purity quartz mineral resource engineering. *J. Mineral. Petrol.* **2012**, *32*, 38–44. [CrossRef]
25. China Technical Committee for Standardization of Microbeam Analysis. *GB/T 15617-2002 Methods for Quantitative Analysis of Silicate Minerals by Electron Probe*; Standards Press of China: Beijing, China, 2002.
26. China Technical Committee for Standardization of Semiconductor Equipment and Materials. *SJ/T 11554-2015 Determination of the Metals' Concentration of Hydrofluoric Acid by ICP-OES*; Standards Press of China: Beijing, China, 2015.
27. China Technical Committee for Standardization of Semiconductor Equipment and Materials. *GB/T 32650-2016 Determining the Content of Trace Elements in Arenaceous Quartz by Inductively Coupled Plasma Mass Spectrometry (ICP-MS)*; Standards Press of China: Beijing, China, 2016.
28. Lei, S.M.; Lin, M.; Pei, Z.Y.; Wang, E.W.; Zang, F.F.; Xiong, K. Occurrence and removal of mineral impurities in quartz. *China Min. Mag.* **2016**, *25*, 79–83. [CrossRef]
29. Shmulovich, K. An experimental study of phase equilibria in the systems H_2O-CO_2-$CaCl_2$ and H_2O-CO_2-NaCl at high pressures and temperatures (500–800 °C, 0.5–0.9 GPa): Geological and geophysical applications. *Contrib. Mineral. Petrol.* **2004**, *146*, 450–462. [CrossRef]
30. Yan, F.L. Distribution properties and hosting conditions and purification methods of baneful impurity elements in quartz. *J. Geol.* **2009**, *33*, 277–279. [CrossRef]
31. Zhang, Z.Z.; Li, J.S.; Li, X.X.; Huang, H.Q.; Zhou, L.F.; Xiong, T.T. High efficiency iron removal from quartz sand using phosphoric acid. *Int. J. Miner. Process.* **2012**, *114–117*, 30–34. [CrossRef]
32. Bai, J.X.; Li, S.Q.; Yang, C.Q.; Kong, J.W. Study on the influence of ultrasound on iron removal by acid leaching for quartz sand. *Nonmet. Mines* **2016**, *39*, 69–71. [CrossRef]
33. Tang, Q.; Sun, X.M.; Xu, L.; Zhai, W.; Liang, J.L.; Liang, Y.H.; Shen, K. U-Th-Pb Chemical dating of monazite exsolutions in apatite aggregates in quartz veins of UHP rocks from the Chinese Continental Scientific Drilling (CCSD) Project. *Acta Petrol. Sin.* **2006**, *22*, 1927–1932.
34. Götze, J. Chemistry, textures and physical properties of quartz-geological interpretation and technical application. *Mineral. Mag.* **2009**, *73*, 645–671. [CrossRef]
35. Mclaren, A.C.; Cook, R.F.; Hyde, S.T.; Tobin, R.C. The mechanisms of the formation and growth of water bubbles and associated dislocation loops in synthetic quartz. *Phys. Chem. Miner.* **1983**, *9*, 79–94. [CrossRef]
36. Zhou, L.G. *The Basic of Ore Petrology*, 3rd ed.; Metallurgical Industry Press: Beijing, China, 2007; pp. 206–309.
37. Liu, C.; Lin, J. Influence of calcination temperature on dielectric constant and structure of the micro-crystalline muscovite. *China Nonmet. Min. Ind. Her.* **2008**, *5*, 38–46. [CrossRef]

38. Liu, X.C.; Wu, Y.B.; Gong, H.J.; Yang, S.H.; Wang, J.; Peng, M.; Jiao, W.F. Zircon age and Hf isotopic composition of quartz veins in UHP eclogites from western Dabie Mountains. *Chin. Sci. Bull.* **2009**, *54*, 1449–1454. [CrossRef]
39. Lu, H.P.; Wang, R.C.; Lu, X.X.; Xu, S.J.; Chen, J.; Gao, J.F. Study on dissolution behavior of zircon in hydrothermal solution of 180 °C. *Prog. Nat. Sci.* **2003**, *13*, 1042–1047. [CrossRef]
40. Schmidt-Mumm, A. Low frequency acoustic emission from quartz upon heating from 90 to 610 °C. *Phys. Chem. Miner.* **1991**, *17*, 545–553. [CrossRef]